Effects of Protein Kinase C Dependent Phosphorylation and a Familial Hypertrophic Cardiomyopathy-Related Mutation of Cardiac Troponin I on Structural Transition of Troponin C and Myofilament Activation†

Tomoyoshi Kobayashi,*,‡ Wen-Ji Dong,§ Eileen M. Burkart,‡ Herbert C. Cheung,§ and R. John Solaro‡

Department of Physiology and Biophysics, Center for Cardiovascular Research, College of Medicine, University of Illinois at Chicago, Chicago, Illinois 60612-7342, and Department of Biochemistry and Molecular Genetics, University of Alabama at Birmingham, Birmingham, Alabama 35294-0005

Received November 19, 2003; Revised Manuscript Received March 3, 2004

ABSTRACT: In experiments reported here, we compared tension and thin filament Ca^{2+} signaling in preparations containing either wild-type cardiac troponin I (cTnI) or a mutant cTnI with an R146G mutation [cTnI(146G)] linked to familial hypertrophic cardiomyopathy. Myofilament function is altered in association with cTnI phosphorylation by protein kinase C (PKC), which is activated in hypertrophy. Whether there are differential effects of PKC phosphorylation on cTnI compared to cTnI(146G) remains unknown. We therefore also studied cTnI and cTnI(146G) with PKC sites mutated to Glu, which mimics phosphorylation. Compared to cTnI controls, binary complexes with either cTnI(146G) or cTnI(43E/45E/144E) had a small effect on Ca^{2+}-dependent structural opening of the N-terminal regulatory domain of cTnC as measured using Förster resonance energy transfer. However, this structural change was significantly reduced in the cTnC−cTnI(43E/45E/144E/146G) complex. Exchange of cTnI in skinned fiber bundles with cTnI(146G) induced enhanced Ca^{2+} sensitivity and an elevated resting tension. Exchange of cTnI with cTnI(43E/45E/144E) induced a depression in Ca^{2+} sensitivity and maximum tension. However, compared to cTnI(146G), cTnI(43E/45E/144E/146G) had little additional effects on myofilament response to Ca^{2+}. By comparing activation of tension to the open state of the N-domain of cTnC with variations in the state of cTnI, we were able to provide data supporting the hypothesis that activation of cardiac myofilaments is tightly coupled to the open state of the N-domain of cTnC. Our data also support the hypothesis that pathological effects of phosphorylation are influenced by mutations in cTnI.

Ca^{2+} regulation of striated muscle contraction involves interactions among proteins of the troponin (Tn)[1] complex (TnC, TnI, and TnT) and tropomyosin (Tm) (*1*−*7*). Ca^{2+} binding to TnC triggers a release of the thin filament from inhibition by an inhibitory region of TnI and a movement of TnT and Tm that promotes the reaction of cross-bridges with actin. In heart muscle, phosphorylation and mutations of cardiac TnI (cTnI) that modify the activation process appear to be of significance in hypertrophy and failure. Depression of myofilament tension and shortening velocity occurs with phosphorylation of cTnI by protein kinase C (PKC) (*8*−*10*), which is activated in the cascade that signals compensatory myocyte growth and leads to decompensation (*11*). Moreover, there are mutations found in cTnI that have been linked to familial hypertrophic cardiomyopathy (FHC) and that culminate in sudden death (*12*−*14*). An important unanswered question is whether effects of PKC-dependent phosphorylation of wild-type cTnI are the same or different in the FHC-related cTnI mutant. In experiments reported here, we have probed effects of FHC-linked mutation (R146G of cTnI; R145G in human cTnI sequence) and PKC-dependent phosphorylation of cTnI, alone and together, on molecular signaling at the interface of cTnI and cTnC and on tension developed by myofilaments.

A primary event in signaling at the interface of TnI and TnC is a Ca^{2+}-dependent structural opening of the N-domain of TnC, which initiates activation of the thin filament. The crystal structures of vertebrate fast skeletal TnC (fsTnC) show two globular domains, each of which contains a pair of Ca^{2+}-binding sites (*15*−*17*). The sites in the N-terminal domain are the regulatory sites and are specific for Ca^{2+}, whereas those in the C-terminal domain bind both Ca^{2+} and Mg^{2+}. One of the regulatory Ca^{2+}-binding sites in cTnC cannot bind Ca^{2+} under the physiological conditions due to the amino acid replacement of the coordinating residue (*18*). Ca^{2+} binding to the regulatory sites of fsTnC results in the opening of the hydrophobic pocket in the N-terminal domain (*17*, *19*). For cTnC to expose its hydrophobic pocket, a

† This work was supported by American Heart Association Scientist Development Grants (0230038N to T.K. and 0330170N to W.-J.D.) and National Institute of Health Grants (R01 HL 64035 and P01 HL 62426 Project 1 to R.J.S. and R01 HL 52508 to H.C.C.). E.M.B. was supported by an American Heart Association (Midwest Affiliate) Pre-Doctoral Fellowship and National Institute of Health Grant T3207692.

* To whom correspondence should be addressed. Tel: 312-996-7151. Fax: 312-996-1414. E-mail: tkoba@uic.edu.

‡ University of Illinois at Chicago.

§ University of Alabama at Birmingham.

[1] Abbreviations: Tn, troponin; cTn, cardiac troponin; Tm, tropomyosin; PKC, protein kinase C; FHC, familial hypertrophic cardiomyopathy; AEDANS, 5-[(iodoacetamidoethyl)amino]naphthalene-1-sulfonic acid; MOPS, 3-(*N*-morpholino)propanesulfonic acid; FRET, Förster resonance energy transfer; HW, half-width (full width at half-maximum).

10.1021/bi036073n CCC: $27.50
Published on Web 04/28/2004

complex formation with the C-terminal part of the inhibitory region of cTnI is required (*20*, *21*). The Ca^{2+}-induced interaction between the hydrophobic pocket of the N-domain of TnC and the C-terminal part of the inhibitory region of TnI triggers the series of conformational transitions among myofilament proteins (e.g., refs *22*−*27*), which results in activation of thin filament.

In experiments reported here, we conducted Förster resonance energy transfer (FRET) experiments in order to assess the effects of PKC-dependent phosphorylation and/or FHC-related mutation of cTnI on the structural opening of the N-terminal domain of cTnC. We used Glu substitution at major PKC-dependent phosphorylation sites on cTnI (Ser-43, Ser-45, and Thr-144) to mimic fully phosphorylated states as we demonstrated recently (*10*). We also measured the effects of these mutations on steady-state tension of detergent-treated mouse cardiac fiber bundles. Our data demonstrate significant differences between effects of PKC pseudophosphorylation of cTnI and cTnI (R146G) on myofilament Ca^{2+} sensitivity and maximum tension as well as the open state of the N-domain of cTnC.

EXPERIMENTAL PROCEDURES

Preparation of Proteins. Recombinant human cardiac troponin C (cTnC) and a mutant cTnC(20W/51C) were expressed in BL21(DE3) cells using the pET3d vector and purified according to the method described previously (*21*, *28*, *29*). The Trp-less mutant (dW) of mouse cTnI(wt) inserted into the pET3d vector (*30*) was created by replacing Trp-192 with Phe using the QuickChange site-directed mutagenesis kit (Stratagene). PKC pseudophosphorylation (S43E/S45E/T144E) and/or FHC-related mutation (R146G) were further introduced into either cTnI(wt) or dW-cTnI(wt). Recombinant cTnIs were expressed and purified as previously described (*25*). Recombinant mouse cardiac troponin T (cTnT) inserted into the pSBET vector was expressed and purified as described (*31*, *32*). The single cysteine in the cTnC mutant [cTnC(20W/51C)] was labeled with IAEDANS in the presence of 6 M urea (*33*), and the degree of labeling was found to be >0.97 mol of probe/mol of protein. Reconstitution of the binary complex with unlabeled or labeled cTnC and cTnI mutants was carried out by following the procedure described in the previous work (*34*). The final step of dialysis was against a working buffer containing 0.15 M KCl, 5 mM $MgCl_2$, 1 mM EGTA, 1 mM dithiothreitol, and 50 mM MOPS at pH 7.0.

Fluorescence Measurements. Steady-state measurements were carried out in a solution containing 0.15 M KCl, 5 mM $MgCl_2$, 1 mM EGTA, 1 mM dithiothreitol, and 50 mM MOPS, pH 7.0 at 20 ± 0.1 °C, on an ISS PC1 photon-counting spectrofluorometer, using a band-pass of 3 nm on both the excitation and emission monochromators (*33*). Emission spectra were corrected for variation of the detector system with wavelength. For each emission spectrum, the background signal was corrected using solutions in which proteins were omitted. Protein concentration was 5 μM for all spectral measurements. When Ca^{2+} was present, the total concentration was 2 mM.

FRET Ca^{2+} titration was carried out on the ISS PC1 equipped with a Micro 4 autotitrator (World Precision) with the excitation wavelength set at 295 nm and the emission wavelength at 333 nm for donor Trp. The titration was sequentially performed on the donor-only labeled protein sample (P-D), followed by measurements on the donor−acceptor labeled protein sample (P-DA) at the same concentration as the P-D sample (*35*). Background tracings were recorded with buffer containing no proteins. Fluorescence intensity was collected by monitoring changes in fluorescence intensity of the tryptophan donor for both P-D (I_D) and P-DA (I_{DA}) samples at 333 nm, and the background was subtracted. The Ca^{2+}-dependent average FRET efficiency, E, was determined from the ratio of the two averaged fluorescence intensity signals from the P-DA and P-D titrations using the equation:

$$E = 1 - I_{DA}/I_D \quad (1)$$

The Ca^{2+}-dependent distance (R) change was then determined using the equation:

$$R = R_0[(1 - E)/E]^{1/6} \quad (2)$$

With eqs 1 and 2, one can generate an experimental measure of FRET efficiency or distance as a function of $[Ca^{2+}]$ for each donor and acceptor pair.

Fluorescence intensity decay was measured at 20 ± 0.1 °C in the time domain with an IBH 5000 photon-counting lifetime system equipped with a very stable flash lamp operated at 40 kHz in 0.5 atm of hydrogen. For determination of FRET, the donor intensity from donor-alone and donor−acceptor samples was collected into 1024 channels of a multichannel analyzer under identical experimental conditions. These decay data were analyzed as a sum of exponential terms to calculate the distribution of the intersite distances using the program CFS_LS/GAUDIS (http://cfs.umbi.umd.edu/index.html) as in previous studies (*33*, *34*). The reduced chi square ratio (χ_R^2) was used to judge goodness of fit for the distribution. For all FRET experiments, the donor was Trp-20 of cTnC and the acceptor was the extrinsic fluorophore AEDANS covalently linked to the single Cys residue at position 51 of cTnC. The excitation and emission wavelengths for Trp were 295 and 333 nm, respectively. For AEDANS the corresponding wavelengths were 330 and 480 nm, respectively. The overlap integral was determined for each experimental condition, using experimental values of the quantum yield and the Förster distance (R_0).

Steady-State Tension Measurements. We measured tension generated by detergent-treated fiber bundles dissected from the left ventricular papillary muscles of mouse hearts as previously described (*10*). Male CD-1 mice (age 3 months) were anesthetized by injection with pentobarbital sodium (50 mg/kg body weight) into the peritoneal cavity. The hearts were quickly excised, and left ventricular papillary muscle fiber bundles were isolated and dissected into strips approximately 150−200 μm in width and 3−4 mm in length at 4 °C. The fiber bundle was then placed in HR solution (53.5 mM KCl, 10 mM EGTA, 25 μM $CaCl_2$, 6.81 mM $MgCl_2$, 5 mM ATP, 12 mM creatine phosphate, 10 units/mL bovine heart creatine kinase, 1 mM dithiothreitol, 1% Triton X-100, and 20 mM MOPS, pH 7.0). The detergent-skinned fiber bundle was mounted between a force transducer and a micromanipulator, and the sarcomere length was

adjusted to 2.3 μm. Initial maximum isometric force was measured in activating solution (pCa 4.5) containing 33.8 mM KCl, 10 mM EGTA, 9.96 mM $CaCl_2$, 5.39 mM ATP, 6.47 mM $MgCl_2$, 12 mM creatine phosphate, 10 units/mL creatine kinase, 1 mM dithiothreitol, and 20 mM MOPS, pH 7.0. Force was measured while the fibers were bathed in sequentially increasing Ca^{2+} concentrations ranging from pCa 8.0 to pCa 4.5. Endogenous Tn was then exchanged as described in Burkart et al. (*10*). The skinned fiber bundles were incubated with an excess of cTnT−cTnI, followed by reconstitution with cTnC. After reconstitution with cTnC, maximum Ca^{2+}-activated force was measured in pCa 4.5 solution, followed by force measurements ranging from pCa 8.0 to pCa 4.5.

TnC−TnI Binding Measurements. The effects of mutations on the interactions of cTnI with cTnC were assessed by surface plasmon resonance spectroscopy using a BIAcore 1000 instrument (BIAcore, Inc., Piscataway, NJ) at 25 °C (*36*, *37*). To immobilize cTnI on a sensor chip, 2-(2-pyridinyldithio)ethanamine was first cross-linked to carboxyl groups of sensor chip C1 by EDC/NHS, and then cTnI was introduced for immobilization through thiol coupling. To analyze the kinetics of the interaction between cTnC and immobilized cTnI, different concentrations of cTnC, ranging from 5 to 250 nM, depending on the analysis, were injected. The analysis was carried out with association times of either 90 or 120 s and a dissociation time of 300 s in 0.3 M NaCl, 5 mM $MgCl_2$, 0.1 mM $CaCl_2$, and 20 mM MOPS, pH 7.0, at a flow rate of either 30 or 50 μL/min. Regeneration of the sensor chips was carried out by injecting 6 M urea, 1 M NaCl, 10 mM EDTA, and 20 mM MOPS, pH 7.0. Control experiments were carried out using a flow cell prepared with the same procedure except that cTnI was omitted. We found no nonspecific binding of cTnC to the sensor chip under our experimental conditions. After the background was subtracted, the data were fit to a two-step binding model (two-state reaction model):

$$A + B \underset{k_{-1}}{\overset{k_{+1}}{\leftrightarrow}} (AB)^* \underset{k_{-2}}{\overset{k_{+2}}{\leftrightarrow}} AB$$

using the global data analysis with the BIAevaluation version 3.1 program. Thus association rate constant $k_{on} = k_{+1}$, dissociation rate constant $k_{off} = k_{-1}k_{-2}/(k_{+1} + k_{+2})$, and association constant $K_a = k_{on}/k_{off}$.

RESULTS

Distance Distribution Analysis. To determine the influence of PKC pseudophosphorylation and/or FHC-related mutations on the ability of cTnI to induce a structural transition in the N-domain of cTnC, we employed FRET measurements between Trp-20 (donor) and AEDANS labeled at Cys-51 (acceptor) of cTnC (*21*, *35*). Trp-20 is located in the A-helix, and Cys-51 is located at the B−C linker. Upon Ca^{2+} binding to the regulatory site(s) of TnC, helices B and C move away from helices A and D. Thus Ca^{2+}-dependent structural opening of the N-terminal domain of cTnC in a binary complex with cTnI can be monitored as a decrease of transfer efficiency by FRET measurements between these two sites.

Figure 1 illustrates the distance distribution with the assumption of Gaussian distribution, and Table 1 summarizes the distance distribution parameters. Lifetime measurements of the donor in the presence and absence of the acceptor allowed us to recover the distance distribution between donor and acceptor (*38*). In a binary complex with dW-cTnI(wt) and cTnC(20W/51C), the mean distance between the donor and acceptor was 15.5 Å, as calculated from distance distribution analysis in the absence of Ca^{2+}. Upon Ca^{2+} binding to the regulatory site and induction of the structural change in the N-terminal domain of cTnC(20W/51C), the mean distance increased to 22.9 Å. These distances and the distance change are in good agreement with our previous measurements (*21*, *35*) and with the distances calculated from NMR structures (*20*, *39*, *40*). As summarized in Table 1, introduction of PKC pseudophosphorylation into dW-cTnI(wt) resulted in a small increase of the mean distance

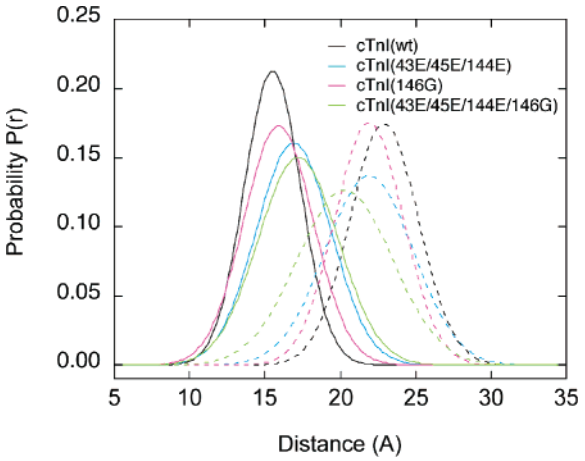

FIGURE 1: Area-normalized distance distribution profiles of the cTnI−cTnC binary complex. The energy donor was Trp-20 of cTnC, and the acceptor was AEDANS attached to Cys-51 of cTnC. The binary complexes contained either dW-cTnI(wt) (black), dW-cTnI(43E/45E/144E) (cyan), dW-cTnI(146G) (magenta), or dW-cTnI(43E/45E/144E/146G) (green). Solid lines and dash lines are Mg^{2+} states and Ca^{2+} states, respectively. Distribution parameters are summarized in Table 1. The experiments were repeated to confirm reproducibility.

Table 1: Distance Distribution Parameters from Fluorescence Lifetime Measurements[a]

dW-cTnI mutation	conditions	mean distance (R/Å)	half-width (HW/Å)	χ_R^2	distance changes (Å)
wt	Mg^{2+}	15.5 (17.5)	4.42	1.05 (2.97)	
	Ca^{2+}	22.9 (20.9)	5.37	1.07 (3.10)	7.4
43E/45E/144E	Mg^{2+}	16.9 (19.0)	5.84	1.10 (5.23)	
	Ca^{2+}	21.9 (19.0)	6.85	1.05 (4.81)	5.0
146G	Mg^{2+}	15.9 (18.0)	5.42	1.06 (14.1)	
	Ca^{2+}	21.9 (19.0)	5.35	1.07 (12.7)	6.0
43E/45E/144E/146G	Mg^{2+}	17.2 (18.0)	6.25	1.09 (3.21)	
	Ca^{2+}	20.3 (19.0)	7.42	1.08 (2.78)	3.1

[a] Intersite distances between Trp-20 of cTnC and AEDANS at Cys-51 of cTnC were measured in a binary complex with one of the cTnI mutants. Experimental conditions were described in Experimental Procedures. Each set of data was refitted by holding the mean distance at the value in parentheses, and the resultant χ_R^2 value is also shown in parentheses.

(1.4 Å) in the absence of Ca^{2+} and a smaller increase of the distance (5.5 Å) induced by Ca^{2+} compared to the binary complex with dW-cTnI(wt). In both the absence and the presence of Ca^{2+}, half-widths (HW) of the distance distributions increased as compared to dW-cTnI(wt). dW-cTnI(146G) had an effect on distance change similar to dW-cTnI(43E/45E/144E). Introduction of the PKC pseudophosphorylation to dW-cTnI(146G) increased the mean distance to 17.2 Å and the HW to 6.25 Å in the absence of Ca^{2+}, but the effect of Ca^{2+} on the distance was an increase of only 3.1 Å, although the distribution was broadened by 1.17 Å. The difference in the mean distance between the absence and presence of Ca^{2+} for this mutation was only ~40% of that observed for dW-cTnI(wt) and ~50% of that for dW-cTnI(146G). The Ca^{2+}-induced increase in HW was ~40% of that observed for dW-cTnI(wt). Thus the combined effects of PKC pseudophosphorylation and FHC-related mutation appeared to be essentially additive.

To examine the extent to which the observed difference between two distributions of distances determined in the absence and presence of Ca^{2+} can be considered distinct, we refitted the data by holding the mean distance at the value shown in parentheses in Table 1. For dW-cTnI(wt), a change of 2 Å resulted in a 3-fold increase in the values of χ_R^2. Larger elevations (5−14-fold) in χ_R^2 were obtained for two of the other three mutants of dW-cTnI. For the third mutant, a change of 1 Å in the mean distance resulted in a 3-fold elevation of the χ_R^2 value. This analysis indicates that the uncertainty of the best fitted values for the mean distances was not likely more than 2 Å and, in each case, the two distributions are distinct.

In general, deviation of the distances in the Mg^{2+} state or Ca^{2+} state from dW-cTnI(wt) was accompanied by an increase of HW, indicating alteration of the equilibrium between the open and closed forms of cTnC, as discussed below. When PKC pseudophosphorylation and/or the FHC-related mutation were introduced into dW-cTnI, the apparent structure of the N-domain of cTnC became more flexible in both the presence and the absence of Ca^{2+}.

In our FRET data analysis to recover the distribution of distances between Trp-20 and Cys-51 of cTnC, several criteria clearly showed distinct distributions of donor−acceptor distances for the complexes reconstituted with different cTnI mutants. The recovered distributions are apparent distributions in that they are influenced by the Förster critical distance (R_0) of the donor−acceptor pair, the orientations of donor and acceptor, and their motions, conformation fluctuation, and site−site diffusion of the protein. In particular, a distribution of the orientation factor (κ^2) can contribute to the overall observed apparent distance distributions. In our calculation of the mean distances from the distribution of the distances, a value of $^2/_3$ was used for the orientation factor κ^2, based on the assumption of isotropic and rapid tumbling of the fluorophores. If this value was inappropriate or different for the different biochemical states, the calculated distances would be subjected to an uncertainty that cannot be quantitatively assessed. There is no theoretical model to predict the exact value of κ^2. However, the potential contribution of the orientation factors can be estimated from the axial depolarization factors of the donor and acceptor (*41*). We measured the anisotropy decays of both the donor and acceptor in each complex reconstituted with different cTnI mutants (data not shown). The limiting anisotropy values derived from the decays were used to calculate their respective axial depolarization factors and the range of κ^2 ($\kappa^2_{min} - \kappa^2_{max}$). These results are listed in Table 2. The range of κ^2 was 0.28−2.1 for all distances. The expected error resulting from the use of a value of $^2/_3$ for the orientation factor to calculate the mean distance is less than 20%. The variations of the axial depolarization factors listed in the Table 2 for either donor or acceptor in different complexes with or without the presence of Ca^{2+} are less than 11%. These results suggest that both fluorophores do not experience significant changes in their orientations upon reconstitution with different cTnI mutants and Ca^{2+} binding. Therefore, much of the observed changes in the mean distance and apparent half-width of the distribution between the donor and acceptor sites could be due to structural dynamic changes of the proteins.

Table 2: Anisotropy Parameters of Tryptophan (Donor) and IAEDANS (Acceptor) in cTnC(20W/51C)−cTnI Complexes[a]

dW-cTnI mutation	conditions	anisotropy[b]		depolarization factor[c]		orientation factor[d]	
		$r_{0,D}$	$r_{0,A}$	$\langle d^X_D \rangle$	$\langle d^X_A \rangle$	κ^2_{min}	κ^2_{max}
wt	Mg^{2+}	0.158	0.141	0.718	0.381	0.200	1.94
	Ca^{2+}	0.165	0.157	0.750	0.424	0.275	2.08
43E/45E/144E	Mg^{2+}	0.151	0.144	0.686	0.389	0.308	1.92
	Ca^{2+}	0.162	0.158	0.736	0.427	0.279	2.07
146G	Mg^{2+}	0.165	0.157	0.75	0.424	0.275	2.07
	Ca^{2+}	0.157	0.149	0.714	0.403	0.294	1.99
43E/45E/144E/146G	Mg^{2+}	0.160	0.147	0.727	0.397	0.292	1.99
	Ca^{2+}	0.155	0.139	0.775	0.376	0.283	2.02

[a] Experimental conditions were the same as those used in Table 1. [b] $r_{0,D}$ and $r_{0,A}$ are limited anisotropy of the donor and acceptor, respectively, and are determined from the respective anisotropy decay curves. [c] $\langle d^X_D \rangle$ and $\langle d^X_A \rangle$ are axial depolarization factors for the donor and acceptor in the protein, respectively, and are calculated as previously described (*41*). [d] κ^2_{min} and κ^2_{max} are the lower and upper limits, respectively, of the orientation factors calculated from $r_{0,D}$ and $r_{0,A}$ (*41*).

Steady-State Fluorescence. To assess the effects of PKC pseudophosphorylation and/or FHC-related mutation of cTnI on Ca^{2+} sensitivity of the structural opening of the N-domain of cTnC, we employed Ca^{2+} titration in the absence and presence of acceptor (AEDANS at Cys-51 of cTnC) and calculated FRET efficiency. Figure 2 shows the pCa−distance relations in a binary complex with each of the recombinant cTnIs. The distance between the donor and acceptor was calculated from FRET efficiency according to eqs 1 and 2. The maximum and minimum distances obtained from these experiments are in good agreement with those obtained from the distance distribution analysis described above. The pCa_{50} values, which correspond to $-\log [Ca^{2+}]$ at which 50% of the distance change occurred, obtained by titrating the distances with Ca^{2+} were 5.41 for dW-cTnI(wt), 5.30 for dW-cTnI(43E/45E/144E), 5.30 for dW-cTnI(146G), and 5.09 for dW-cTnI(43E/45E/144E/146G). Both 146G and 43E/45E/144E mutations reduced the pCa_{50} value by 0.11 pCa unit compared to the dW-cTnI(wt). The 43E/45E/144E/146G mutation reduced the pCa_{50} value by 0.32 pCa unit compared to the dW-cTnI(wt).

Figure 5A shows the relationship between pCa_{50} values obtained from steady-state fluorescence experiments and the mean distances and distance changes obtained from FRET measurements. The data show a clear correlation between

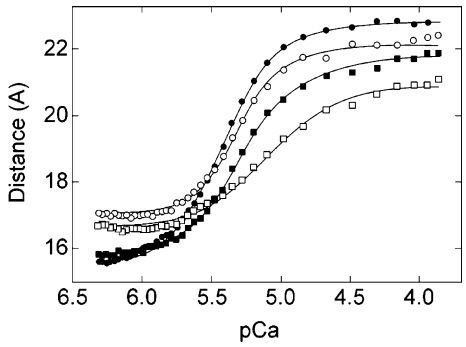

FIGURE 2: FRET-sensed Ca^{2+} titration of the cTnI−cTnC binary complex. The complexes contained either dW-cTnI(wt) (closed circle), dW-cTnI(43E/45E/144E) (open circle), dW-cTnI(146G) (closed square), or dW-cTnI(43E/45E/144E/146G) (open square). Trp at position 20 (donor) of cTnC was excited at 295 nm, and emission was recorded at 333 nm. AEDANS attached to Cys-51 of cTnC was the acceptor. FRET efficiency was converted to distance as described in Experimental Procedures. The data were fitted with a simple Hill equation. pCa_{50} (Hill coefficient) values obtained from these experiments were 5.41 (2.19) for dW-cTnI(wt), 5.30 (2.58) for dW-cTnI(43E/45E/144E), 5.30 (2.05) for dW-cTnI(146G), and 5.09 (1.77) for dW-cTnI(43E/45E/144E/146G). The experiments were repeated to confirm reproducibility.

the Ca^{2+} sensitivity and distance changes. This indicates significant energy coupling between Ca^{2+} binding and the structural transition in the cTnC−cTnI binary complex.

Tension Measurements. To assess functional effects of recombinant cTnIs [cTnI(wt), cTnI(43E/45E/144E), cTnI(146G), and cTnI(43E/45E/144E/146G)] and their dW-cTnI counterparts, as well as the cTnC mutant [cTnC(20W/51C)], we measured the isometric tension of detergent-treated (skinned) fiber bundles, in which the endogenous cTn complex was exchanged with each of the recombinant cTn complexes. The results are summarized in Figure 3 and Table 3.We first replaced the endogenous cTn ternary complex with the cTnT−cTnI binary complex, and the whole cTn complex was then reconstituted by adding cTnC (*10*, *31*). Alkali−urea polyacrylamide gel electrophoresis verified the absence of cTnC following extraction (data not shown). The slower mobility of recombinant cTnT, which contained a myc tag at its N-terminus, permitted determination of cTnT exchange. Using an anti-TnT antibody, we determined the extent of Tn replacement by Western blot analysis (Figure 3A). When we exchanged the endogenous Tn complex with the recombinant Tn complex containing cTnI(wt) or cTnI(S43E/S45E/T144E), we were able to replace nearly 100% of the Tn complex with the exogenous Tn complex, whereas 80−90% of the native Tn complex was exchanged with Tn complexes with the R146G mutation.

Panels B and C of Figure 3 show the pCa−tension relations, and Figure 3D shows maximum and minimum tensions for fiber bundles where endogenous cTn was replaced by one of the recombinant cTn complexes. Compared to fiber bundles with dW-cTnI(wt), fiber bundles that contained dW-cTnI(43E/45E/144E) were desensitized to Ca^{2+}, whereas fiber bundles that contained dW-cTnI(146G) were sensitized to Ca^{2+} (Figure 3B). Furthermore, compared to fiber bundles with dW-cTnI(wt), those with dW-cTnI(43E/45E/144E) showed a reduction of maximum tension. However, introduction of the R146G mutation resulted in an increased maximum tension and a significantly increased minimum tension (Figure 3D). Qualitatively, these

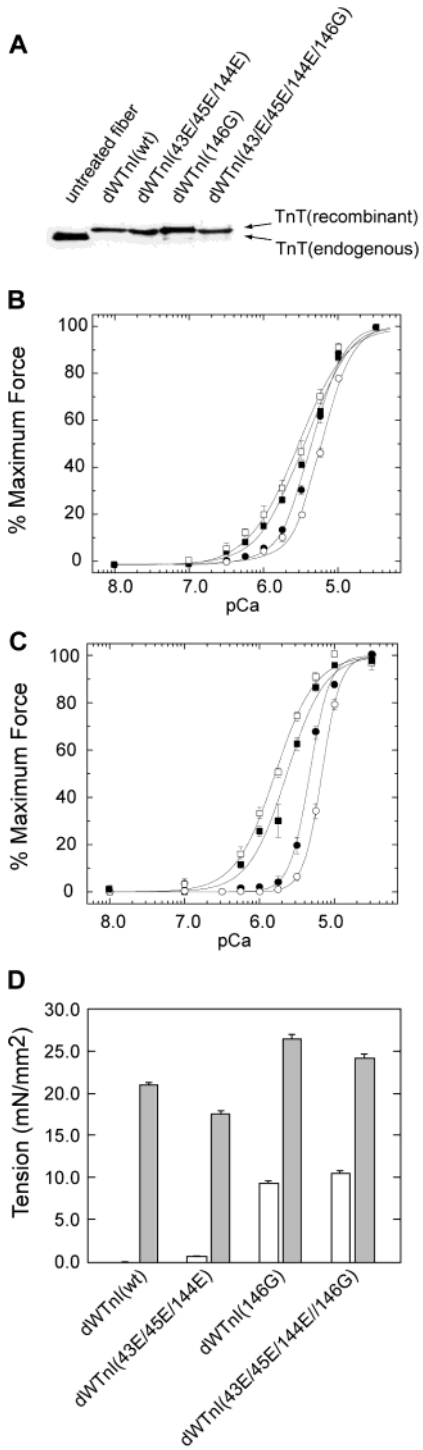

FIGURE 3: Effects of cTnI mutations on force−pCa relation of skinned fiber bundles. The endogenous cTn complex was replaced by treatment with the cTnT−cTnI complex followed by addition of cTnC to reconstitute the whole cTn complex as described previously (*21*, *31*). (A) Western blot analysis of cTnT using an anti-TnT antibody to estimate the exchange efficiency. Since the recombinant TnT has a c-myc tag at its N-terminus, it shows slower mobility compared to endogenous cTnT. (B) Force−Ca^{2+} relations for skinned fiber bundles containing dW-cTnI(wt) (filled circles), dW-cTnI(43E/45E/144E) (open circles), dW-cTnI(146G) (filled squares), or dW-cTnI(43E/45E/144E/146G) (open squares). The Tn complex was reconstituted by adding cTnC(20W/51C). (C) Force−Ca^{2+} relations for skinned fiber bundles containing cTnI(wt) (filled circles), cTnI(43E/45E/144E) (open circles), cTnI(146G) (filled squares), or cTnI(43E/45E/144E/146G) (open squares). The ternary Tn complex was reconstituted by adding cTnC. (D) Maximum and minimum tensions for skinned fiber bundles containing dW-cTnIs.

Table 3: Summary of Results from Skinned Fiber Studies[a]

cTnI	pCa_{50}	Hill coeff	max tension (mN/mm^2)	min tension (mN/mm^2)
wt	5.33 ± 0.01	3.25 ± 0.30	23.02 ± 0.49	1.37 ± 0.25
S43E/S45E/T144E	5.17 ± 0.01	3.51 ± 0.35	13.77 ± 0.06	0.00 ± 0.02
R146G	5.63 ± 0.03	1.70 ± 0.12	30.11 ± 1.33	6.25 ± 0.82
S43E/S45E/T144E/R146G	5.79 ± 0.02	1.64 ± 0.11	26.90 ± 0.96	7.45 ± 0.77
dW/wt	5.37 ± 0.01	2.12 ± 0.12	21.10 ± 0.41	0.00 ± 0.18
dW/S43E/S45E/T144E	5.25 ± 0.02	2.09 ± 0.14	17.57 ± 0.43	0.70 ± 0.16
dW/R146G	5.46 ± 0.02	1.46 ± 0.10	26.58 ± 0.65	9.48 ± 0.26
dW/S43E/S45E/T144E/R146G	5.54 ± 0.03	1.38 ± 0.11	24.06 ± 0.62	10.59 ± 0.27

[a] Endogenous cTnI in detergent-skinned fiber bundles was exchanged with various mutant forms of recombinant cTnI, and the effects on Ca^{2+} sensitivity (pCa_{50}), cooperativity (Hill coefficient), and tension development (maximum and minimum) were determined. The numbers were expressed as mean ± SEM from eight to twelve fibers (three to four mice).

observations are consistent with the data from fiber bundles without the dW (Trp-192 to Phe) mutation of cTnI and the 20W/51C mutation of cTnC as shown in Figure 3C. Thus the effects of PKC pseudophosphorylation on the activity of myofilaments are dependent on whether residue 146 of cTnI is Arg (wt) or Gly (FHC-related mutant).

In Figure 5B, we show the extent of muscle activation defined as (maximum tension) − (minimum tension) as a function of the relation between apparent Ca^{2+} affinity derived from the tension measurement or from Ca^{2+} titration using steady-state fluorescence measurements. There was a weak correlation between muscle activation and apparent Ca^{2+} affinity for tension development (closed circle), whereas there was a strong correlation between muscle activation and the apparent Ca^{2+} affinity for the structural transition in the cTnC−cTnI binary complex (open squares).

Interaction between TnC and TnI. The interaction of cTnC with immobilized cTnI was analyzed in real time using surface plasmon resonance spectroscopy (BIAcore). In our experiments, to avoid the artifacts (such as mass-transport effect, steric hindrance, or nonspecific binding of the analyte to the sensor chip), purified cTnI was immobilized on a C1 chip by thiol coupling, and experiments were conducted with relatively low surface density of the ligand and high flow rate (*42*). To maintain the solubility of cTnI, we used 0.3 M NaCl for the running buffer. The interaction of cTnI with cTnC was analyzed in the presence of 5 mM $MgCl_2$ and 0.1 mM $CaCl_2$, pH 7.0 at 25 °C. Two examples of sensograms are shown in Figure 4, and kinetic parameters obtained by global fit to a two-step binding model are summarized in Table 4. The R146G mutation of cTnI resulted in a decreased association rate constant (k_{on}), whereas PKC pseudophosphorylation resulted in an increase of the dissociation rate constant (k_{off}). PKC pseudophosphorylation of cTnI(wt) increased the dissociation rate constant 17-fold, resulting in a 20-fold lower affinity for cTnC. PKC pseudophosphorylation of cTnI(R146G) also induced a faster dissociation rate constant (22-fold) and lower affinity (32-fold) for cTnC.

Only a two-step binding model could fit our data reasonably. This is not surprising considering the multiple interaction sites between TnC and TnI (*43*, *44*). Recently, Tripet et al. reported the interaction between fsTnC and several peptides derived from the inhibitory region and the regulatory region of fsTnI using the SPR technique (*45*). The data thus obtained should be simpler than those between whole proteins. Interestingly, they also found that a two-step binding model was required to fit their data. Although one might speculate that each step (fast or slow) in the association and

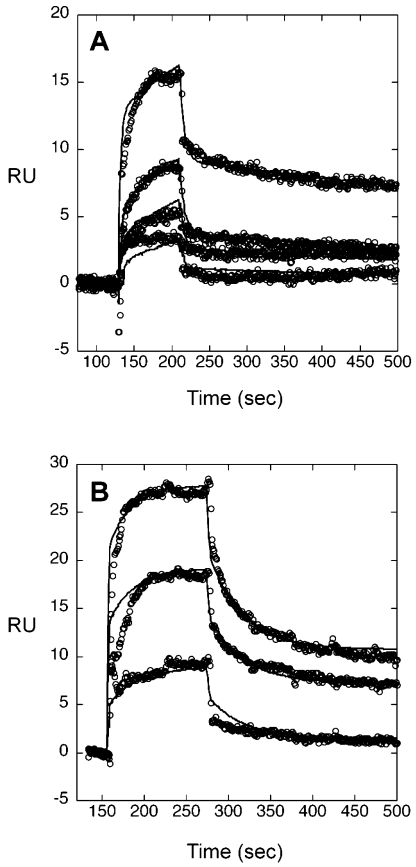

FIGURE 4: Interaction of cTnC with wild-type (A) and PKC pseudophosphorylated (B) cTnI determined by surface plasmon resonance. cTnI was immobilized on a sensor chip, and varied concentrations of cTnC were injected over the surface as described in Experimental Procedures. Injection was performed for 90 s (A) or 120 s (B) followed by 300 s of dissociation phase at a flow rate of 50 μL/min in these cases. Concentrations of cTnC injected were (A) 114.3, 57.2, 28.6, and 14.3 nM (from top) and (B) 245, 123, and 61 nM (from top). R_{max} (density of immobilized cTnI on the surface chip) values were (A) 21.5 RU and (B) 30.1 RU, respectively. Solid lines indicate fitted curves according to the two-step binding model.

Table 4: Summary of Affinities and Rate Constants for cTnC Binding to Immobilized cTnIs[a]

cTnI	k_{on} ($M^{-1}\,s^{-1}$)	k_{off} (s^{-1})	K_a (M^{-1})
wt	1.59×10^6	1.54×10^{-2}	1.03×10^8
S43E/S45E/T144E	1.40×10^6	2.64×10^{-1}	5.30×10^6
R146G	2.80×10^5	8.00×10^{-3}	3.50×10^7
S43E/S45E/T144E/R146G	1.90×10^5	1.76×10^{-1}	1.08×10^6

[a] The affinities between cTnC and immobilized cTnIs were measured by BIAcore surface plasmon resonance. The solution conditions were 0.3 M NaCl, 5 mM $MgCl_2$, 0.1 mM $CaCl_2$, and 20 mM MOPS, pH 7.0 at 25 °C. In all cases, standard errors for the fitted parameters (k_{+1}, k_{-1}, k_{+2}, and k_{-2}) were 5−15% of the fitted values. The values k_{on}, k_{off}, and K_a were calculated as described in Experimental Procedures.

dissociation phases corresponds to sequential binding of TnI to the N- and C-domain of TnC, this interpretation requires more investigation. In general, clearer determination of the relationship between kinetic parameters and the structural information awaits further experiments.

DISCUSSION

Our data provide novel and important evidence on the mechanism of activation of cardiac myofilaments and how this mechanism is modified by TnI charge modifications associated with FHC and posttranslational modifications. By comparing activation of tension to the open state of the N-domain of cTnC with variations in the state of cTnI, we were able to provide data supporting the hypothesis that activation of cardiac myofilaments is tightly coupled to the open state of the N-domain of cTnC. Both PKC pseudophosphorylation and a missense mutation of cTnI induced alterations in the open state of cTnC. Moreover, the apparent Ca^{2+} affinity of this structural transition in a binary complex, not apparent Ca^{2+} affinity for fiber bundles, correlated well with isometric tension activation of skinned fiber bundles. Our data demonstrating that effects of PKC pseudophosphorylation of cTnI on tension and the open state of the N-terminus of cTnC are significantly altered in an FHC-related mutant of cTnI are also of importance to our understanding of regulation of myocardial contraction in physiological and pathological states.

Evidence on the crystal structure of the core domain of the cTn complex provides a rationale for the effects of charge modification of the PKC sites on cTnI (*46*). Two of the PKC phosphorylation sites, Ser-43 and Ser-45, are located in the N-terminal α-helical region of cTnI [H1(I)]. Although the N-terminal half of H1(I) interacts with the C-lobe of cTnC extensively, close examination of the crystal structure of the core domain of the cTn complex revealed that there is no interaction between Ser-43 or Ser-45 with the C-domain of cTnC; rather Ser-45 of cTnI may interact with Glu-10 in the N-domain of cTnC. Thus PKC phosphorylation of Ser-45 may disrupt the interaction with Glu-10 of cTnC and have direct impact on the Ca^{2+} binding to the regulatory site of cTnC. This is intriguing considering the recent NMR measurements that detected a structural disruption at the N-cap position of the G-helix in the C-domain of cTnC, rather than residue(s) in the N-domain, by replacement of Ser-43 and Ser-45 of cTnI with Asp both in a cTnI−cTnC binary complex and in a cTnT−cTnI−cTnC ternary complex (*47*). Another PKC phosphorylation site, Thr-144, and FHC-related mutation site we are investigating, Arg-146, are located in the minimum inhibitory region of cTnI. The minimum inhibitory region (residues 138−149 of cTnI) by itself is able to interact with actin and inhibit actin-activated myosin ATPase activity. In the crystal structure of the core domain of the cTn complex (*46*), the minimum inhibitory region was not visible, indicative of the flexible structure of this region in the complex. This was also indicated by a spin-labeling EPR experiment (*48*). Studies by Dong et al. (*29*) detected the structural transition of the inhibitory region by measuring of the distance between the N-terminus and the C-terminus of this region, which increased upon Ca^{2+} binding to the regulatory site of cTnC both in the cTnC−cTnI binary complex and in the cTn ternary complex. We also measured the various distances among cTnI and modeled the structural change of the inhibitory region and the following regulatory region of cTnI (*49*). Yet the precise structural mechanism by which PKC pseudophosphorylation and/or the FHC-related mutation introduced into cTnI affect(s) the structural transition of the N-domain of cTnC and its transduction to other thin filaments remained to be established.

There are previous reports describing mutations that induce alteration in the Ca^{2+}-binding property of TnC (e.g., refs *50*−*55*). For example, the replacement of the Ca^{2+}-coordinating Glu residue at the −Z position of the E-F hand Ca^{2+}-binding site I of fsTnC to Ala resulted in the loss of Ca^{2+}binding to the site (*40*). da Silva et al. (*56*) were able to increase Ca^{2+}-binding affinity by mutating hydrophobic residues that are exposed upon Ca^{2+} binding to less hydrophobic residues. Another example reported recently involved the replacement of hydrophobic residues that buried in the apo state to less hydrophobic amino acids (*57*). In these latter two cases changes in the stability of either the Ca^{2+}-bound or apo state of TnC induced altered Ca^{2+}-binding affinity. Another way to alter Ca^{2+}-binding affinity is by manipulating the interaction with a target protein (*58*). In this study, by introducing PKC pseudophosphorylation and/or FHC-related mutation into cTnI, we were able to change the apparent Ca^{2+}-binding property of cTnC. This effect appeared to be derived from the alteration of binding affinity between cTnC and cTnI as shown in Figure 4 and Table 4.

Despite the number of reports describing the alteration of Ca^{2+}-binding affinity of cTnC as mentioned above, the structural consequence of changing the Ca^{2+}-binding affinity of cTnC remains unknown. Gagné et al. (*59*) reported that the N-domain of fsTnC with replacement of the −Z position of the Ca^{2+}-binding site I to Ala remained as a closed form even after binding Ca^{2+} to site II. However, to the best of our knowledge, ours is the first report that describes the partial structural opening of the N-domain of TnC by altering the Ca^{2+}-binding properties. It should be mentioned that what we observed here are average distances derived from distance distribution analysis under certain conditions. If there are only two structural states (open and closed states) in the N-domain of cTnC, an observed shift of a distribution along the distance axis may be interpreted as the shift of the equilibrium between closed and open states. Interestingly, all of the mutations we investigated in this study caused a shift of structural equilibrium in both the presence and the absence of Ca^{2+} at the single regulatory site of cTnC in the cTnC−cTnI complex. The only exception was the single mutant R146G mutation in the presence of Ca^{2+} (Table 1).

It is apparent that PKC pseudophosphorylation and/or FHC-related mutation affect the distribution among three states of thin filaments by altering the equilibrium between the open and closed state of the N-domain of cTnC. There is evidence that thin filaments exist in a dynamic equilibrium among three states (blocked, closed, and open states). In diastole (low [Ca^{2+}] conditions), the state of cardiac thin filaments is believed to be 50% in a blocked state and 40% in a closed state (*60*). Upon Ca^{2+} binding to the regulatory site in cTnC, the equilibrium changes to one in which 75% of thin filaments are in the closed state and 20% are in an open state. As shown in Figure 3, the introduction of the R146G mutation into cTnI(wt) or cTnI(43E/45E/144E) resulted in the increase of minimum tension caused by incomplete turning off of cross-bridge cycling. This indicates

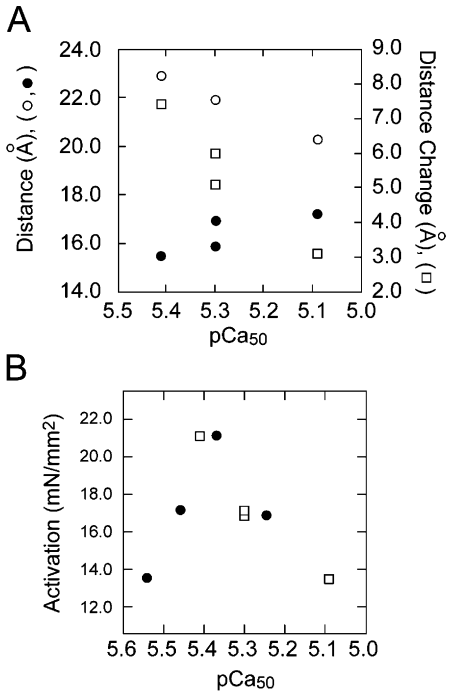

FIGURE 5: Correlation between pCa_{50} and distance change in the N-domain of cTnC and between pCa_{50} and muscle activation. (A) Distance and distance change−pCa_{50} relationship. pCa_{50} values were taken from steady-state fluorescence titration (Figure 2). Distances in the Mg^{2+} state (closed circles) and Ca^{2+} states (open circles) and distance changes (open squares) were obtained from distance distribution analysis (Table 1). (B) Muscle activation−pCa_{50} relationship. Muscle activation was defined as (maximum tension) − (basal tension) determined by steady-state tension measurements (Figure 3D). pCa_{50} values were taken from steady-state fluorescence titration (open squares, Figure 2) and skinned fiber tension measurements (closed circles, Table 2). Note that muscle activation correlates well with pCa_{50} values from fluorescence titration (open square) but not with pCa_{50} values from tension measurements (closed circle).

that the R146G mutation may shift the equilibrium from the blocked state to the closed and open states in diastole. This is intriguing because whereas the 43E/45E/144E/146G mutation affected the mean distance between the donor and acceptor the most and increased the distance between the donor and acceptor in the Mg^{2+} state, the R146G mutation caused minimum effect on the mean distance in the Mg^{2+} state. This effect, however, must be attributed to the alteration of actin−cTnI interaction rather than alteration of the cTnC−cTnI interaction, since, as mentioned above, the R146G mutation is located in the inhibitory region of cTnI, which interacts with actin in the absence of Ca^{2+} and inhibits actin-activated myosin ATPase activity. It should also be mentioned that mutation at position 146 of cTnI affects cooperative activation of the myofilaments (Figure 3 and Table 3).

The most interesting finding in the present study is that the muscle activation, defined as (maximum tension) − (minimum tension), correlates well with pCa_{50} values obtained from FRET titration, not pCa_{50} values from tension measurements, as shown in Figure 5B. As mentioned above, pCa_{50} values obtained from FRET titration also correlate with the structural opening of the regulatory N-terminal domain of cTnC. Thus the extent of muscle activation was determined by the extent of structural opening of cTnC, which was altered by mutations introduced into cTnI. This is intriguing because whereas TnI has been known as an inhibitor of actin−myosin interaction, modification of TnI may also function to determine the degree of muscle activation.

REFERENCES

1. Ebashi, S., and Endo, M. (1968) Calcium ion and muscle contraction, in *Progress in Biophysics and Molecular Biology* (Butler, A. V., and Noble, D., Eds.) pp 123−183, Pergamon Press, Oxford.
2. Leavis, P. C., and Gergely, J. (1984) Thin filament proteins and thin filament-linked regulation of vertebrate muscle contraction, *CRC Crit. Rev. Biochem. 16*, 235−305.
3. Zot, A. S., and Potter, J. D. (1987) Structural aspects of troponin-tropomyosin regulation of skeletal muscle contraction, *Annu. Rev. Biophys. Biophys. Chem. 16*, 535−559.
4. Farah, C., and Reinach, F. C. (1995) The troponin complex and regulation of muscle contraction, *FASEB J. 9*, 755−767.
5. Tobacman, L. S. (1996) Thin filament-mediated regulation of cardiac contraction, *Annu. Rev. Physiol. 58*, 447−481.
6. Gordon, A. M., Homsher, E., and Regnier, M. (2000) Regulation of contraction in striated muscle, *Physiol. Rev. 80*, 853−924.
7. Solaro, R. J. (2001) Modulation of cardiac myofilament activity by protein phosphorylation, in *Handbook of Physiology: Section 2: The Cardiovascular System, Vol. 1, The Heart* (Page, E., Fozzard, H., and Solaro, R. J., Eds.) pp 264−300, Oxford University Press, New York.
8. Noland, T. A. Jr., and Kuo, J. F. (1993) Protein kinase C phosphorylation of cardiac troponin I and troponin T inhibits Ca^{2+}-stimulated MgATPase activity in reconstituted actomyosin and isolated myofibrils, and decreases actin-myosin interactions, *J. Mol. Cell. Cardiol. 25*, 53−65.
9. Noland, T. A., Jr., Guo, X., Raynor, R. L., Jideama, N. M., Averyhart-Fullard, V., Solaro, R. J., and Kuo, J. F. (1995) Cardiac troponin I mutants, *J. Biol. Chem. 270*, 25445−25454.
10. Burkart, E. M., Sumandea, M. P., Kobayashi, T., Nili, M., Martin, A. F., Homsher, E., and Solaro, R. J. (2003) Phosphorylation or glutamic acid substitution at protein kinase C sites on cardiac troponin I differentially depress myofilament tension and shorting velocity, *J. Biol. Chem. 278*, 11265−11272.
11. Molkentin, J. D., and Dorn, G. W., II (2001) Cytoplasmic signaling pathway that regulate cardiac hypertrophy, *Annu. Rev. Physiol. 63*, 391−426.
12. Kimura, A., Harada, H., Park, J. E., Nishi, H., Satoh, M., Takahashi, M., Hiroi, S., Sasaoka, T., Ohbuchi, N., Nakamura, T., Koyanagi, T., Hwang, T. H., Choo, J. A., Chung, K. S., Hasegawa, A., Nagai, R., Okazaki, O., Nakamura, H., Matsuzaki, M., Sakamoto, T., Toshima, H., Koga, Y., Imaizumi, T., and Sasazuki, T. (1997) Mutations in the cardiac troponin I gene associated with hypertrophic cardiomyopathy, *Nat. Genet. 16*, 379−382.
13. Redwood, C. S., Moolman-Smook, J. C., and Watkins, H. (1999) Properties of mutant contractile proteins that cause hypertrophic cardiomyopathy, *Cardiovasc. Res. 44*, 20−36.
14. Hernandez, O. M., Housmans, P. R., and Potter, J. D. (2001) Pathophysiology of cardiac muscle contraction and relaxation as a result of alterations in thin filament regulation, *J. Appl. Physiol. 90*, 1125−1136.
15. Herzberg, O., and James, M. N. G. (1985) Structure of the calcium regulatory muscle protein troponin-C at 2.8 Å resolution, *Nature 313*, 653−659.
16. Sundaralingam, M., Bergstrom, R., Strasburg, G., Rao, S. T., Roychowdhury, P., Greaser, M., and Wang, B. C. (1985) Molecular structure of troponin C from chicken skeletal muscle at 3-angstrom resolution, *Science 227*, 945−948.
17. Houdusse, A., Love, M. L., Dominguez, R., Grabarek, Z., and Cohen, C. (1997) Structures of four Ca^{2+}-bound troponin C at 2.0 Å resolution, *Structure 5*, 1695−1711.
18. Collins, J. H. (1991) Myosin light chains and troponin C: structural and evolutionary relationships revealed by amino acid sequence comparisons, *J. Muscle Res. Cell Motil. 12*, 3−25.
19. Slupsky, C. M., and Sykes, B. D. (1995) NMR solution structure of calcium-saturated skeletal muscle troponin C, *Biochemistry 34*, 15953−15964.
20. Li, M. X., Spyracopoulos, L., and Sykes, B. D. (1999) Binding of cardiac troponin-I147−163 induces a structural opening in human cardiac troponin-C, *Biochemistry 38*, 8289−8298.

21. Dong, W.-J., Xing, J., Villain, M., Hellinger, M., Robinson, J. M., Chandra, M., Solaro, R. J., Umeda, P. K., and Cheung, H. C. (1999) Conformation of the regulatory domain of cardiac muscle troponin C in its complex with cardiac troponin I, *J. Biol. Chem. 274*, 31382−31390.
22. Tao, T., Gong, B.-J., and Leavis, P. C. (1990) Calcium-induced movement of troponin-I relative to actin in skeletal muscle thin filaments, *Science 247*, 1339−1341.
23. Miki, M. (1990) Resonance energy transfer between points in a reconstituted skeletal muscle thin filament, *Eur. J. Biochem. 187*, 155−162.
24. Vibert, P., Craig, R., and Lehman, W. (1997) Steric-model for activation of muscle thin filaments, *J. Mol. Biol. 266*, 8−14.
25. Kobayashi, T., Kobayashi, M., Gryczynski, Z., Lakowicz, J. R., and Collins, J. H. (2000) Inhibitory region of troponin I: Ca^{2+}-dependent structural and environmental changes in the troponin-tropomyosin complex and in reconstituted thin filaments, *Biochemistry 39*, 86−91.
26. Kobayashi, T., Kobayashi, M., and Collins, J. H. (2001) Ca^{2+}-dependent, myosin subfragment 1-induced proximity changes between actin and the inhibitory region of troponin I, *Biochim. Biophys. Acta 1549*, 148−154.
27. Hai, H., Sano, K.-I., Maeda, K., Maéda, Y., and Miki, M. (2002) Ca^{2+}- and S1-induced conformational changes of reconstituted skeletal muscle thin filaments observed by fluorescence energy transfer spectroscopy, *J. Biochem. 131*, 407−418.
28. Kobayashi, T., Zhao, X., Wade, R., and Collins, J. H. (1999) Ca^{2+}-dependent interaction of the inhibitory region of troponin I with acidic residues in the N-terminal domain of troponin C, *Biochim. Biophys. Acta 1430*, 214−221.
29. Dong, W.-J., Xing, J., Robinson, J. M., and Cheung, H. C. (2001) Ca^{2+} induces an extended conformation of the inhibitory region of troponin I in cardiac muscle troponin, *J. Mol. Biol. 314*, 51−61.
30. Guo, X., Wattanapermpool, J., Palmiter, K. A., Murphy, A. M., and Solaro, R. J. (1994) Mutagenesis of cardiac troponin I, *J. Biol. Chem. 269*, 15210−15216.
31. Chandra, M., Kim, J. J., and Solaro, R. J. (1999) An improved method for exchanging troponin subunits in detergent skinned rat cardiac fiber bundles, *Biochem. Biophys. Res. Commun. 263*, 219−223.
32. Sumandea, M. P., Pyle, W. G., Kobayashi, T., de Tombe, P. P., and Solaro, R. J. (2003) Identification of a functionally critical protein kinase C phosphorylation residue of cardiac troponin T, *J. Biol. Chem. 278*, 35135−35144.
33. She, M., Xing, J., Dong, W.-J., Umeda, P. K., and Cheung, H. C. (1998) Calcium binding to the regulatory domain of skeletal muscle troponin C induces a highly constrained open conformation, *J. Mol. Biol. 281*, 445−452.
34. Dong. W.-J., Wang, C. K., Gordon, A. M., Rosenfeld, S. S., and Cheung, H. C. (1997) A kinetic model for the binding of Ca^{2+} to the regulatory site of troponin from cardiac muscle, *J. Biol. Chem. 272*, 19229−19235.
35. Dong, W.-J., Robinson, J. M., Xing, J., and Cheung, H. C. (2003) Kinetics of conformational transitions in cardiac troponin induced by Ca^{2+} dissociation determined by Forster resonance energy transfer, *J. Biol. Chem. 278*, 42394−42402.
36. Schuck, P. (1997) Use of surface plasmon resonance to probe the equilibrium and dynamic aspects of interactions between biological macromolecule, *Annu. Rev. Biophys. Biomol. Struct. 26*, 541−566.
37. Myszka, D. G. (2000) Kinetic, equilibrium, and thermodynamic analysis of macromolecular interactions with BIACORE, *Methods Enzymol. 323*, 325−340.
38. Lakowicz, J. R., Gryczynski, I., Cheung, H. C., Wang, C.-K., Johnson, M. L., and Joshi, N. (1988) Distance distributions in proteins recovered by using frequency-domain fluorometry, *Biochemistry 27*, 9149−9160.
39. Sia, S. K., Li, M. X., Spyracopoulos, L., Gagné, S. M., Liu, W., Putkey, J. A., and Sykes, B. D. (1997) Structure of cardiac muscle troponin C unexpectedly reveals a closed regulatory domain, *J. Biol. Chem. 272*, 18216−18221.
40. Li, M. X., Gagné, S. M., Spyracopoulos, L., Kloks, C. P. A. M., Audette, G., Chandra, M., Solaro, R. J., Smillie, L. B., and Sykes, B. D. (1997) NMR studies of Ca^{2+} binding to the regulatory domains of cardiac and E41A skeletal muscle troponin C reveal the importance of site I to energetics of the induced structural changes, *Biochemistry 36*, 12519−12525.
41. Dale, R. E., Eisinger, J., and Blumberg, W. E. (1979) The orientational freedom of molecular probes, *Biophys. J. 26*, 161−194.
42. Myszka, D. G. (1999) Improving biosensor analysis, *J. Mol. Recognit. 12*, 279−284.
43. Kobayashi, T., Grabarek, Z., Gergely, J., and Collins, J. H. (1995) Extensive interactions between troponin C and I: zero-length cross-linking of troponin I and acetylated troponin C, *Biochemistry 34*, 10946−10952.
44. Ferrières, G., Pugnière, M., Mani, J.-C., Villard, S., Laprade, M., Doutre, P., Pau, B., and Granier, C. (2000) Systematic mapping of regions of human cardiac troponin I involved in binding to cardiac troponin C, *FEBS Lett. 479*, 99−105.
45. Tripet, B., de Crescenzo, G., Grothe, S., O'Connor-McCourt, M., and Hodges, R. S. (2002) Kinetic analysis of the interactions between troponin C and the C-terminal troponin I regulatory region and validation of a new peptide delivery/capture system used for surface plasmon resonance, *J. Mol. Biol. 323*, 345−362.
46. Takeda, S., Yamashita, A., Maeda, K., and Maéda, Y. (2003) Structure of the core domain of human cardiac troponin in the Ca^{2+}-saturated form, *Nature 424*, 35−41.
47. Finley, N. L., Ward, D. G., Trayer, I. P., and Rosevear, P. R. (2003) *Biophys. J. 84*, 566a.
48. Brown, L. J., Sale, K. L., Hills, R., Rouviere, C., Song, L., Zhang, X., and Fajer, P. G. (2002) Structure of the inhibitory region of troponin by site directed spin labeling electron paramagnetic resonance, *Proc. Natl. Acad. Sci. U.S.A. 99*, 12765−12770.
49. Dong, W.-J., Robinson, J. M., Stagg, S., Xing, J., and Cheung, H. C. (2003) Ca^{2+}-induced conformational transition in the inhibitory and regulatory regions of cardiac troponin I, *J. Biol. Chem. 278*, 8686−8692.
50. Putkey, J. A., Sweeney, H. L., and Campbell, S. T. (1989) Site-directed mutation of the trigger calcium-binding sites in cardiac troponin C, *J. Biol. Chem. 264*, 12370−12378.
51. Grabarek, Z., Tan, R.-Y., Wang, J., Tao, T., and Gergely, J. (1990) Inhibition of mutant troponin C activity by an intra-domain disulphide bond, *Nature 345*, 132−135.
52. Fujimori, K., Sorenson, M., Herzberg, O., Moult, J., and Reinach, F. C. (1990) Probing the calcium-induced conformational transition of troponin C with site-directed mutants, *Nature 345*, 182−184.
53. Golosinska, K., Pearlstone, J. R., Borgford, T., Oikawa, K., Kay, C. M., Carpenter, M. R., and Smillie, L. B. (1991) Determination of and corrections to sequences of turkey and chicken troponins-C, *J. Biol. Chem. 266*, 15797−15809.
54. Trigo-Gonzalez, G., Awang, G., Racher, K., Neden, K., and Borgford, T. (1993) Helix variants of troponin C with tailored calcium affinities, *Biochemistry 32*, 9826−9831.
55. Leblanc, L., Bennet, A., and Borgford, T. (2000) Calcium affinity of regulatory sites in skeletal troponin-C is attenuated by N-cap mutations of helix C, *Arch. Biochem. Biophys. 384*, 296−304.
56. da Silva, A. C., de Araujo, A. H. B., Herzberg, O., Moult, J., Sorenson, M., and Reinach, F. C. (1993) Troponin-C mutants with increased calcium affinity, *Eur. J. Biochem. 213*, 599−604.
57. Tikunova, S. B., Rall, J. A., and Davis, J. P. (2002) Effect of hydrophobic residue substitutions with glutamine on Ca^{2+} binding and exchange with the N-domain of troponin C, *Biochemistry 41*, 6697−6705.
58. Ward, D. G., Brewer, S. M., Cornes, M. P., and Trayer, I. A. (2003) A cross-linking study of the N-terminal extension of human cardiac troponin I, *Biochemistry 42*, 10324−10332.
59. Gagné, S. M., Li, M. X., and Sykes, B. D. (1997) Mechanism of direct coupling between binding and induced structural change in regulatory calcium binding proteins, *Biochemistry 36*, 4386−4392.
60. Maytum, R., Westerdorf, B., Jaquet, K., and Geeves, M. A. (2003) Differential regulation of the actomyosin interaction by skeletal and cardiac troponin isoforms, *J. Biol. Chem. 278*, 6696−6701.

BI036073N